Available online at www.sciencedirect.com
SCIENCE DIRECT®
Physics of the Earth and Planetary Interiors xxx (2004) xxx–xxx
PHYSICS OF THE EARTH AND PLANETARY INTERIORS
www.elsevier.com/locate/pepi

Evolution of helium and argon isotopes in a convecting mantle

Shunxing Xie [a,*], Paul J. Tackley [a,b]

[a] *Department of Earth and Space Sciences, University of California, Los Angeles, CA 90095, USA*
[b] *Institute of Geophysics and Planetary Physics, University of california, Los Angeles, CA 90095, USA*

Received 9 March 2003; received in revised form 7 October 2003; accepted 27 April 2004

Abstract

Outgassing of helium and argon and the isotope ratio distribution of helium isotopes in basalts are some of the most important geochemical constraints on mantle structure and evolution, but their interpretation in terms of mantle processes is ambiguous and controversial. Here, the evolution of these isotopes and their radiogenic parent isotopes of U, Th and K are studied using a numerical model of mantle convection that combines a treatment of major and trace element melting-induced differentiation and evolution with a self-consistent mantle convection-plate tectonics treatment. Both olivine and pyroxene-garnet system phase transformations are included, with density profiles of the different components following established data up to 720 km depth, but varied in the deeper mantle to reflect present uncertainties. Cases are presented that focus on the influence of two uncertain physical parameters: the density of subducted eclogite in the deep mantle, and the partition coefficient for helium. Results indicate that the system self-consistently evolves regions with the observed range of $^3He/^4He$, but the exact distribution depends strongly on physical parameters. Furthermore, the distribution depends on sampling method, with the distribution in erupted material often being different from mantle-averaged distributions. Some parameter combinations simultaneously lead to MORB-like distributions of $^3He/^4He$ ratios in erupted material, and ∼50% outgassing of radiogenic ^{40}Ar consistent with geochemical constraints. MORB-like $^3He/^4He$ histograms are produced in erupted material either when the shallow mantle has a high proportion of residue that evolves MORB-like $^3He/^4He$ due to the high incompatibility of He, or when sufficient recycled crust mixes back into the shallow mantle to suitably reduce its $^3He/^4He$. Outgassing is also studied for Venus and Mars-like models, both of which are found to outgas substantially despite their lack of plate tectonics. The 25% outgassing of Venus proposed by [W.M. Kuala. Icarus, 139(1) (1999) 32] is plausible if Venus' mantle viscosity is high or melt does not efficiently degass. It is estimated that Mars has lost ∼90% of its outgassed Ar to space, consistent with other estimates.

Keywords: Planetary outgassing; Radiogenic isotopes; Mantle convection

1. Introduction

1.1. Helium and argon in the Earth's mantle

The noble gases represent excellent natural tracers for sources and migration of volatiles in the Earth's crust, mantle and atmo-hydrosphere. The state of noble gases within Earth's mantle can be studied by analyzing mantle derived materials, such as volcanic rocks, volcanic gases, and mantle xenoliths, which trapped mantle noble gases. During the past decades, noble gas information has been obtained from mid-ocean ridge basalts and ocean island basalts. Although there has been some progress in this field, noble gas isotopes are still the most difficult and weakest area in isotope geochemistry, mainly because

* Corresponding author. Tel.: +1 310 397 8566; fax: +1 310 825 2779/397 8566.
E-mail address: sxie@ess.ucla.edu (S. Xie).

0031-9201/$ – see front matter © 2004 Elsevier B.V. All rights reserved.
doi:10.1016/j.pepi.2004.04.003

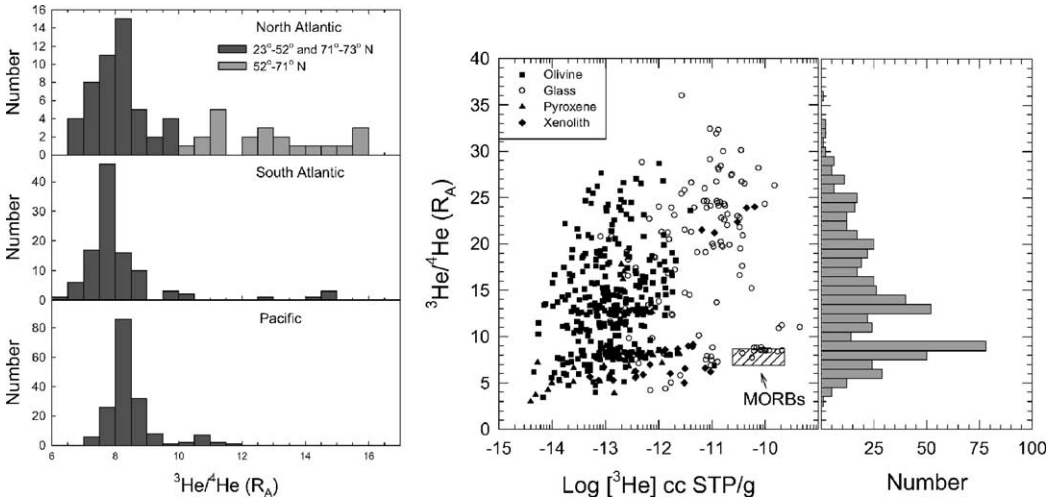

Fig. 1. (A) He isotope ratios in mid-ocean ridge basalt (MORB) glasses. (B) He isotope ratios in ocean island basalts (OIBs) and relationship to ^{3}He concentration. Figures are adapted from Farley and Neroda (1998). Reprinted with permission, from the Annual Review of Earth and Planetary Sciences, vol. 26 ©1998 by Annual Reviews, http://www.annualreviews.org.

of the difficulties in obtaining useful data with high precision.

Observational data from noble gas isotopes impose strong constraints on mantle convection models. According to meteoritic measurements, primordial values of ^{3}He/^{4}He are in the range of 1.4–3.0 $\times 10^{-4}$, or about 100–200 R_a (Jeffrey and Anders, 1970; Craig and Lupton, 1981), where R_a (the atmospheric value of ^{3}He/^{4}He) is 1.38×10^{-6} (Kurz et al., 1983). Over the history of the Earth, the ratio has decreased over time due to radiogenic ingrowth of ^{4}He from U and Th decay. Elemental fractionation between He and U, Th upon melting and outgassing to the atmosphere also have first-order effects on isotope ratio distributions. Thus the present-day distribution of He isotope ratios reflects a combination of ingrowth, fractionation and outgassing.

Histograms of these distributions for mid-ocean ridge basalts (MORBs) and ocean island basalts (OIBs) (Fig. 1) show clear differences. MORBs have a relatively constant ^{3}He/^{4}He ratio with a mean value of 1.16×10^{-5}, which is a factor of 8.4 higher than the atmospheric value (Kurz et al., 1983; Allègre et al., 1995). The range of ^{3}He/^{4}He ratios between 7 and 9 is thus taken as characteristic of the depleted upper mantle. Prominent exceptions are the higher values in the vicinity of Iceland (52°–71°N) and the Easter micro-plate, which are attributed to the involvement of a plume-derived component.

OIB ^{3}He/^{4}He ratios are, in contrast, extremely heterogeneous, extending to both higher and lower values than MORB, although the prominent histogram peak at the MORB value suggests that the depleted upper mantle plays an important role in OIB helium budget. The relationship between ^{3}He/^{4}He and ^{3}He (Fig. 1(B)) indicates very weak, if any, correlation between the ^{3}He/^{4}He ratio and the concentration of ^{3}He. Basalts from the Loihi Seamount are amongst those with the highest ratios, with ^{3}He/^{4}He $= 3.34 \times 10^{-5}$, or about 35 R_a (Kurz et al., 1983). The source of these basalts with high ^{3}He/^{4}He is still controversial, and is one focus of this paper.

Another inert gas of interest is argon. There is almost virtually no primordial ^{40}Ar in the Earth (Ozima and Kudo, 1972), it being entirely produced by the decay of ^{40}K. ^{40}Ar in Earth's atmosphere represents the amount of argon degassed from the Earth's interior, because argon does not escape to the space due to its heavy atomic mass. The atmospheric ^{40}Ar budget implies that approximately half of all ^{40}Ar produced within Earth since its formation is retained within the solid Earth (Allègre et al., 1996), although this figure is rather uncertain, mainly because the amount of ^{40}K in the mantle is uncertain; for example, estimates of K/U range from a widely-accepted

value of 12,700 (Jochum et al., 1983) to as low as 2800(Stacey, 1992). Another more problematic constraint is that the inferred concentration of argon in the MORB source is much lower than what would be expected if the ^{40}Ar remaining in the mantle were evenly distributed (Turner, 1989), which has been interpreted to mean that the additional, 'missing' ^{40}Ar must be 'hidden' somewhere in the lower mantle (Allègre et al., 1996), although this difficulty could be resolved if the amount of ^{40}K in the mantle were lower than commonly estimated (Albarède, 1998; Davies, 1999). This, as well as two other major noble gas paradoxes, could be reconciled if the estimate of ^{40}Ar in the shallow mantle, which comes from measured short-term ^{3}He fluxes into the oceans, were too low by a factor of 3.5(Ballentine et al., 2002). Argon isotope ratios do not receive a lot of interest but are here summarized for completeness: The present isotope ratio for the atmosphere is ^{40}Ar/^{36}Ar = 295.5. The value for MORB ^{40}Ar/^{36}Ar ranges from slightly above the atmospheric value to 40,000 (Allègre et al., 1983; Farley and Neroda, 1998). At the other extreme, a sample from the Loihi Seamount has ^{40}Ar/^{36}Ar = 400–4000 (Hiyagon et al., 1992). However, the differences in ^{40}Ar/^{36}Ar between MORB and OIB have been dimishing, e.g., ^{40}Ar/^{36}Ar ratios in Samonan xenoliths range from 300 to 15,000 (Burnard et al., 1998). All OIB have gone through source outgassing and contamination before eruption so it is difficult to infer argon isotope ratios in the source region.

In summary, helium and argon data impose severe constraints on models of mantle structure and evolution, which must be able to answer questions such as: Where exactly is the high ^{3}He/^{4}He material? Can the required isotope ratio distributions be generated by recycling, or is primordial material necessary? If there is a primitive helium or argon "reservoir", how can it survive for billions of years in the presence of efficient mantle mixing? To satisfy both helium and argon constraints, a mantle convection model must be able to generate a ^{3}He/^{4}He distribution that is Earth-like, and to outgas about 50% of its ^{40}Ar.

1.2. Argon constraints on Mars and Venus

The Venusian atmospheric abundance of ^{40}Ar, $3.3(\pm1.1) \times 10^{-9}$ of planet mass (von Zahn et al., 1983), indicates that only 24(±10)% (Kaula, 1999) of the radiogenic argon has escaped from the mantle (assuming K/U of 7220(±1220), which is the average of Venera samples, with a primordial U mantle abundance of 21(±3) ppb, which is the same as Earth's), which contrasts with 52(±9)% for Earth (Allègre et al., 1996). This reduced outgassing efficiency has been attributed to the generally-assumed dryness of Venus' upper mantle and crust, which would result in higher viscosity (other things being equal), or to the rigid lid convection mode of Venus, which may result in lower rate of surface volcanism and outgassing than Earth's plate tectonics convection.

Mars' volatile system is much more complex than Earth's or Venus'. Taking ^{36}Ar = 2.71×10^{-13} kg/kg-planet (Pepin, 1991), ^{40}Ar/^{36}Ar = 3.01×10^{3} (Sasaki and Tajika, 1994), it is estimated that the ^{40}Ar concentration in the Martian atmosphere is about 0.65 ppb. Taking a terrestrial potassium concentration, and assuming that the loss of radiogenic ^{40}Ar from the Martian atmosphere is negligible (Turcotte and Schubert, 1988), it is estimated that only about 3% ^{40}Ar degassed from the interior of the Martian mantle during the past 4.6 billions years, which is surprisingly low. However, Martian atmospheric volatiles are capable of being lost to space by thermal or non-thermal mechanisms. The noble gases Ar and He can be lost to space because of the impact of O^{+} ions and the solar wind (Jakosky and Jones, 1997). The isotopic data for Ar, C, and H all require the loss of at least half, and more likely, 90%, of the initial inventory of each gas (Jakosky and Jones, 1997). Hutchins and Jakosky (1996) estimated that 85–95% of the ^{36}Ar and 70–88% of the ^{40}Ar has been lost from the atmosphere of Mars. If the fraction of ^{40}Ar that has been lost is assumed to be 90%, the outgassed fraction is increased to about 30–40%.

1.3. Is helium "primordial"?

There is no consensus on how the Earth's mantle obtained material with a high ^{3}He/^{4}He ratio, as sampled, for example, at Hawaii. However, the most common interpretation is that this component comes from an undegassed, 'primitive' source, because noble gases are highly incompatible and volatile, and are thus expected to enter any melt and be heavily out-

gassed prior to or during eruption (Allègre et al., 1983; Farley et al., 1992; Porcelli and Wasserburg, 1995) (note that outgassing requires CO_2 bubbling, which occurs at depths less than 60 km). The need to keep this hypothesized undegassed, high $^3He/^4He$ material intact for billions of years has been used as evidence for a layered mantle, conflicting with various types of geophysical evidence (e.g., reviewed in Tackley, 2000a). One problem with the primitive helium reservoir hypothesis is the question of how such a reservoir could survive for the whole history of the Earth in the face of mantle stirring if, as geophysical evidence implies, convection is basically mantle-wide.

Another possible interpretation of "primordial" helium is that it comes from the core (Porcelli and Halliday, 1992). However, measurements of noble gas partitioning between silicate melt and iron melt under pressures up to 100 kilobars indicate that the partition coefficients are much less than unity and that they decrease systematically with increasing pressure (Matsuda et al., 1993). These results suggest that Earth's core contains only negligible amounts of noble gases if core separation took place under equilibrium conditions at high pressure.

Anderson (1993) suggested that a large amount of ^3He could be delivered to the Earth's surface by cosmic dust, and then recycled to the mantle. Although Anderson's hypothesis has great theoretical appeal, more observations and detailed study of the whole process are needed to fully support it.

Recently it has been argued that high $^3He/^4He$ could be associated with recycled depleted lithosphere (Anderson, 1998; Coltice and Ricard, 1999, 2002; Ferrachat and Ricard, 2001). The latter three studies showed that high $^3He/^4He$ is preserved if residuum can be stored for substantial time periods while the rest of the mantle becomes substantially outgassed. Tackley and Xie (2002) presented two preliminary thermo-chemical convection models that provide some insight into such processes, finding that high $^3He/^4He$ can be generated by recycling residue if He is more compatible than U and Th (e.g. Graham et al., 1990), so that He ratios are frozen in the residuum at the time of melting. However, if was found that the resulting high $^3He/^4He$ residue tends to aggregate near the top (due to its buoyancy) where it should be sampled by mid-ocean ridge volcanism. It was also found that if primitive material exists as a dense basal layer, it must be much denser than subducted crust in order that its primitive (e.g., high ^3He) signature is not swamped by rapid ^4He ingrowth in the U-enriched, He-degassed recycled crust. This line of investigation is further pursued here.

Extreme compositional heterogeneity of the mantle, reminiscent of the "marble cake" proposal of (Allègre and Turcotte, 1986), is a common theme in recent attempts to explain mantle geochemistry. In the marble cake of (Coltice and Ricard, 2002), strips of former oceanic lithosphere carry the high $^3He/^4He$ component and radial stratification is proposed to account for different MORB and OIB signatures. In contrast, Meibom et al. (2003), Meibom and Anderson (2003) proposed that the difference between MORB and OIB is not related to different source regions but is entirely due to different statistical sampling of a highly heterogeneous source region, the Statistical Upper Mantle Assemblage. If this is correct, then the use of He isotopic signature as a fingerprint of plume components is not justified. Helffrich (2002) focused on the role of strips of subducted oceanic crust and supporting seismological observations of mantle heterogeneity.

1.4. Previous relevant numerical modeling

Several other previous numerical modeling studies have given important insight into relevant issues, including the ability (or otherwise) of primitive material to survive over geological time, the possibility of layered convection due to mantle phase transitions, and the evolution of noble gases in a convecting system.

The evolution of noble gases in a mantle that included outgassing and radiogenic ingrowth but not major-element differentiation was investigated by Van Keken and Ballentine (1998, 1999). These studies investigated various proposed mechanisms for maintaining a relatively undegassed lower mantle over billions of years, finding that neither high deep-mantle viscosity, a strongly endothermic phase transition at 660 km depth, or temperature-dependent viscosity, are capable of causing a relatively undegassed deep mantle, in contrast to earlier modeling at lower convective vigor (Gurnis and Davies, 1986). They did find that the observed total amount of ^{40}Ar outgassing is consistent with whole-mantle convection over geological history:

a layered mantle is not required. While the issue of 'primitive' signatures was not resolved, the compositional heterogeneity considered was purely passive, i.e., was not associated with buoyancy variations.

The helium ratio evolution caused by subduction of differentiated oceanic plates was studied by Ferrachat and Ricard (2001), who tracked the evolution of oceanic crust and residue and showed that if oceanic crust segregates at the CMB, a large region of recycled oceanic lithosphere with high ^{3}He/^{4}He can form above it. However, in their model compositional variations were also purely passive, not influencing the flow.

The present paper investigates the possibility that active (buoyant) compositional variations caused by crustal production may play an important role in the evolution of noble gas isotopes and the generation and maintenance of distinct reservoirs. A recent modeling study by Samuel and Farnetani (2003) focused on whether the deep layer proposed by Kellogg et al. (1999) could supply the high ^{3}He/^{4}He component. Here the alternative possibility that He ratios can be generated from a homogeneous start condition (i.e., with no layering) is considered.

An important influence in mantle convection models is the endothermic spinel to perovskite + magnesiowustite phase transition at around 660 km depth, which may cause some partial layering of the convection, and possibly a filtering of chemical anomalies (Weinstein, 1992). However, published models have assumed that the mantle is made of 100% olivine and its high pressure phases, whereas it is well known that the garnet-pyroxene system accounts for at least 40% of the mantle. Phase changes in the latter system occur over a wider depth range, and the equivalent '660' transition was thought to have a neutral or even positive Clapeyron slope, leading to the expectation that it would dilute or even act against the dynamical effect of the endothermic olivine-spinel transition (Weidner and Wang, 1998). Furthermore, when compositional effects are considered, subducted oceanic crust is likely to be buoyant in the depth range 660–720 km (Ringwood, 1990; Ono et al., 2001). Thus, it seems important to take this into account when performing models that include compositional variations associated with oceanic crust and lithosphere. The presented models include these.

2. Model and method

2.1. Physical model

A two-dimensional (2D) cylindrical geometry is assumed (Tackley and Xie, 2002, 2003) with the core size scaled to give the same ratio of CMB surface area to outer surface area as in spherical geometry (Van Keken, 2001). The infinite Prandtl number and compressible anelastic approximations are made (Tackley, 1996a). The equations, nondimensionalized to the mantle depth (D), thermal diffusion time-scale (D^2/κ, where κ = thermal diffusivity) and super-adiabatic drop, $\Delta T_{\rm sa}$, are those of continuity:

$$\nabla(\bar{\rho}\boldsymbol{v}) = 0 \tag{1}$$

conservation of momentum:

$$\nabla\left[\eta\left(v_{i,j}+v_{j,i}-\tfrac{2}{3}v_{k,k}\delta_{ij}\right)\right]-\nabla p = \frac{Ra\hat{z}_i\rho(C,z,T)}{\Delta\rho_{\rm thermal}} \tag{2}$$

conservation of energy:

$$\bar{\rho}\bar{C}_p\frac{DT}{Dt} = -Di_{\rm s}\bar{\alpha}\bar{\rho}Tv_z+\nabla(\bar{k}\nabla T) + \bar{\rho}H+\frac{Di_{\rm s}}{Ra}\eta\left(v_{i,j}+v_{j,i}-\frac{2}{3}v_{k,k}\delta_{ij}\right)v_{i,j} + \bar{C}_p\frac{Di_{\rm s}T}{\bar{\rho}}\sum_{i=1}^{\rm nphase}f_iP_i\frac{d\Gamma_i}{dz}v_z \tag{3}$$

and conservation of bulk chemistry:

$$\frac{\partial C}{\partial t}+\boldsymbol{v}\nabla C = 0 \tag{4}$$

where the surface dissipation number $Di_{\rm s}$ is given by:

$$Di_{\rm s} = \frac{\alpha_{\rm s}gD}{Cp_{\rm s}} \tag{5}$$

and reference Rayleigh number Ra is given by:

$$Ra = \frac{\rho_{\rm s}g\alpha_{\rm s}\Delta T_{\rm sa}D^3}{\eta(T_{\rm as},0)\kappa_{\rm s}} \tag{6}$$

The variables are temperature T, composition C, velocity $\boldsymbol{v}$ and pressure p. The governing parameters are Rayleigh number Ra, internal heating rate H,

Table 1
Thermodynamic parameters for Earth

Parameter	Symbol	Value	Units	Non-D value
Input nondimensional parameters				
Reference Ra	Ra_s	–	–	$1.3(1.0, 0.1) \times 10^7$
Surface dissipation	Di_s	–	–	1.18 (1.01, 0.31)
Mean dissipation	$\langle Di_s \rangle$	–	–	0.38 (0.35,0.18)
Surface Gruneisen	γ_s	–	–	1.1
Nominal dimensional parameters				
Depth of mantle	D	2890 (2742, 2000)	km	1.0
Superadiabatic				
Temperature drop	ΔT_{sa}	2500	K	1.0
Temperature:surface	T_s	300 (700, 200)	K	0.12 (0.28, 0.08)
Expansivity:surface	α_s	5.0×10^{-5}	K^{-1}	1.0
Conductivity:surface	k_s	3.0	W/m/K	1.0
Heat capacity	C_p	1200	J/Kg/K	1.0
Density:surface	ρ_s	3300	Kg/m^3	1.0
Reference viscosity	η_{ref}	1.0(1.0, 1.63)	10^{22} Pa s	1.0
Yield stress	σ_{yield}	100 (–, –)	MPa	1.1 (–, –)$\times 10^5$

Values in parenthesis are for Venus and Mars, respectively.

and surface dissipation number Di_s. Material properties with overbars (density $\bar{\rho}$, thermal expansivity $\bar{\alpha}$, and thermal conductivity $\bar{k}$) vary with depth only, specific heat capacity C_p is constant, $\Delta\rho_{\text{thermal}}$ is the fractional density variation with temperature ($\alpha_{\text{dimensional}} \Delta T_{\text{dimensional}}$) and $\rho(C, z, T)$ is discussed later in Eq. (13)). $\hat{z}$ is a unit vector in the vertical direction, g is the gravitational acceleration and T_{as} is the surface temperature of the reference adiabat. Chemical diffusion is neglected, which corresponds to an infinite Lewis number $Le = \kappa / C_f$, where C_f is the chemical diffusivity. For the ith phase change, P_i is the usual phase buoyancy parameter (Christensen and Yuen, 1985; Tackley et al., 1994), f_i is the fraction of the relevant component in the assemblage and Γ_i is (depth-dependent) phase function. f_i and Γ_i are detailed in Section 2.3.2. Numerically, adiabatic effects resulting from vertical motion (heating/cooling and latent heat) are dealt with by advecting potential temperature, rather than by coding the terms in Eq. (3), as this avoids problems that might result from steep gradients in, for example, Γ_i.

Table 1 lists assumed parameters for Earth, Venus, and Mars. H is not listed in Table 1 because it depends on the concentration of heat producing elements, which varies with position and time, and is thus calculated for each timestep and grid cell as discussed in Section 2.3.4. A thermodynamic model is used to calculate the depth variation of material properties density $\bar{\rho}$, thermal expansivity $\bar{\alpha}$, and thermal conductivity $\bar{k}$, as detailed in previous papers (Tackley, 1996a, 1998; Tackley and Xie, 2003).

Viscosity η depends on temperature and vertical coordinate z:

$$\eta(T, z) = \eta_0 \mathrm{e}^{-(T - T_{0\eta})E_\eta + (z - z_{0\eta})V_\eta} \times [1 + 9H(0.7716 - z)] \quad (7)$$

where E_η and V_η are chosen to give a factor of 10^6 viscosity change between (nondimensional) $T = 0$ and $T = 1$, and a factor of 10^2 increase between the surface and the CMB, in addition to the factor of 10 increase at 660 km depth given by the last term (H is the Heaviside step function). η_0 is set such that $\eta(T_{0\eta}, z_{0\eta}) = 1.0$, where $T_{0\eta} = 0.64$ (dimensional 1600 K) and $z_{0\eta} = 0$. Such strong temperature-dependence gives rigid lid convection (e.g. Moresi and Solomatov, 1995; Solomatov and Moresi, 1996) which is appropriate for the Venus and Mars models, but for studying Earth, a constant yield stress (~100 MPa) is introduced for the top 20% of the domain, which represents ductile, semi-brittle processes and leads to a rudimentary form of plate-like behavior (Tackley, 2000b,c). This yielding is implemented using an effective viscosity, defined as

$$\eta_{\text{eff}} = \min\left[\eta(T,z), \frac{\sigma_{\text{yield}}}{2\dot{\epsilon}}\right] \tag{8}$$

where $\dot{\epsilon}$ is the second invariant of the strain rate tensor:

$$\dot{\epsilon} = \sqrt{\tfrac{1}{2}\dot{\epsilon}_{ij}\dot{\epsilon}_{ij}} \tag{9}$$

The equations are solved using the finite-volume multigrid code STAG3D, as extensively used previously (e.g. Tackley, 1996a, 2000b,c), with 256 evenly-spaced cells in the azimuthal direction and 64 unevenly-spaced cells (giving refinement in the boundary layers) in the radial direction. Compositional variations are tracked using tracer particles, as detailed in (Tackley, 2002; Tackley and King, 2003), with the addition that each tracer carries a certain mass (number of atoms) of each trace element. Compressibility does not require any special tracer treatment, because when moving to regions of higher or lower density, tracers will automatically get closer together or further apart (due to convergence or divergence of the velocity field) by the amount needed to maintain a uniform tracer density per mass of mantle, hence concentration of trace elements. Approximately 400,000 tracers are used, averaging 25 per grid cell.

2.2. Boundary conditions and core cooling

Top and bottom boundaries are impermeable, free-slip and isothermal, while side boundaries are periodic (Venus, Mars cases) or reflecting (Earth cases). Cooling of the core due to heat conducted into the mantle is accounted for using a simple model in which the CMB temperature decreases as heat is removed. (Van Keken, 2001) showed that the CMB heat flux in a cylindrical model with rescaled core radius is essentially the same as that in a spherical model with the normal core radius; thus we here assume a spherical core with the correct radius. The core is assumed to be always in internal thermodynamic equilibrium (has infinite effective thermal conductivity) and homogeneous (i.e., using mean parameters for inner and outer core). The dimensional equation solved for the core's parameterized cooling is (Steinbach and Yuen, 1994):

$$r_c \rho_c C_c \frac{\mathrm{d}T_c}{\mathrm{d}t} = -3q_c \tag{10}$$

where ρ_c denotes mean core density (approximately 11,000 kg/m^3), C_c specific heat (approximately 5×10^2 J kg^{-1} K^{-1}), T_c temperature and q_c heat flux from the core, and r_c core radius (3.485×10^6 m).

After nondimensionalizing the above equation to the standard scales given earlier, the following form is obtained:

$$\mathrm{d}T_n = -\frac{3q_n}{r_n \rho_n C_n}\mathrm{d}t_n \tag{11}$$

where the subscript n denotes nondimensionalized value. Using $r_n = 1.2059$, $\rho_n = 3.3$, $C_n = 0.42$ yields

$$\mathrm{d}T_n = -\frac{q_n}{0.5575}\mathrm{d}t_n \tag{12}$$

2.3. Chemical model

2.3.1. Major elements and melting

Both major and trace elements are tracked in the model, which is designed to represent the mantle-oceanic plate system, i.e, continents are not present. For major elements, a two-component system is assumed, the end-members being crust/eclogite and harzburgite. The variable C, which varies from 0 to 1, represents the fraction of crustal material present, and is initialized at $C = 0.3$ everywhere. Oceanic crust is formed self-consistently by melting and differentiation, which occurs as a separate substep to solving Eqs. (1)–(4), as in previous studies (Tackley and Stevenson, 1993; Scott and Stevenson, 1989). After timestepping Eq. (3), the temperature in some cells may exceed the solidus, which is here based on a fit to experimental data (Zerr et al., 1998; Herzberg et al., 2000) and is composition-independent, except that no melting can occur once the basaltic component has been completely removed (i.e., $C = 0$). The melting substep occurs in these super-solidus cells and involves generating, where sufficient basalt fraction exists, the fraction of partial melt f that brings the temperature back to the solidus, i.e., $f = \min[(T - T_{\text{sol}}(z))/L, C]$ and $T \rightarrow T - Lf$, where L is the latent heat, here assumed to be constant at nondimensional 0.2, corresponding to 600 kJ/kg. The melt is then instantly removed and deposited at the surface to form crust. With this approach, residue from melting is depleted only by the amount needed to generate the formed crust; it is not necessarily $C = 0$ harzburgite. Chemical density variation de-

Table 2
Phase transition properties for Earth, Venus, and Mars

#	Depth (km)	T (K)	$\Delta\rho$ (kg/m^3)	γ (MPa/K)
Olivine system				
1	410 (450, 1081)	1600	280	+2.5
2	660 (730, 1740)	1900	400	−2.5
Pyroxene-garnet system				
c1	60 (70, 158)	0	350	0
2	400 (440, 1055)	1600	150	+1.0
3	720 (800, 1899)	1900	500	+1.0

Depth values in parenthesis are the equivalent depths of phase transition on Venus and Mars. γ is the Clapeyron slope.

pends on depth and composition with both olivine and garnet-pyroxene phase changes implemented, as discussed in the next section.

2.3.2. Multiple phase transitions

A simple parameterization is implemented based on mineral physics data (e.g. Ringwood, 1990; Ono et al., 2001). Minerals are divided into the olivine system and the pyroxene-garnet (px-gt) system, which undergo different phase transitions (Table 2). Therefore, the mixture of minerals depends on composition, pressure (due to solid–solid phase transitions), and temperature (due to their finite Clapeyron slopes). The chemical composition C is mapped linearly into the fraction of the different phase systems, with $C = 1$ (basalt) corresponding to pure px-gt and $C = 0$ (harzburgite) corresponding to 6/7 olivine and 1/7 px-gt. Thus, the olivine fraction $f_{\rm ol} = 6/7(1 - C)$. For calculating mean density it is assumed that the systems can be added linearly, leading to (Tackley and Xie, 2003):

$$\rho(f_{\rm ol}, z, T) = [f_{\rm ol}\bar{\rho}_{\rm olivine}(z, \bar{T}) + (1 - f_{\rm ol})\bar{\rho}_{\rm px-gt}(z, \bar{T})] \times [1 - \alpha_{\rm eff}(T - \bar{T}(z))\Delta\rho_{\rm thermal}] \quad (13)$$

where the $\bar{\rho}(z, T)$ terms depend on depth and the last term accounts for thermal expansion and phase change buoyancy. $\bar{T}(z)$ is the reference adiabat (1600 K potential temperature). The calculation of the reference state density profile is fully detailed in (Tackley, 1996a), the only extension being the addition of density jumps at the phase transition depths, as in (Tackley, 1998).

Table 3
Heat-producing elements

Isotope	Heat (μ W/kg)	Decay rate
^{238}U	95.0	1.55×10^{-10}/year
^{235}U	562.0	9.85×10^{-10}/year
^{232}Th	26.6	4.95×10^{-11}/year
^{40}K	30.0	5.54×10^{-10}/year

The effective thermal expansivity due to phase transitions is an extension of that used in previous studies (e.g. Christensen and Yuen, 1985) and is given by:

$$\alpha_{\rm eff} = \bar{\alpha}(z) + \sum_{i=1}^{\rm nphase} f_i P_i \frac{{\rm d}\Gamma_i}{{\rm d}z} \quad (14)$$

where, for the ith phase change, P_i is the phase buoyancy parameter, f_i is the fraction of the relevant component in the assemblage (= $f_{\rm ol}$ for olivine phase transitions and $(1 - f_{\rm ol})$ for pyroxene-garnet phase transitions) and Γ_i is the phase function, which varies from 0 above a phase transition to 1 below it. Here, the "sheet mass anomaly" approximation is used (Tackley et al., 1994; Tackley, 1996b), which is equivalent to Γ changing from 0 to 1 linearly across one fixed vertical grid level, such that the mass anomalies are concentrated into that grid level.

The density profile of the px-gt component is not well constrained through the lower mantle, with some authors suggesting that it may become less dense than the pyrolite composition at high pressure (e.g. Ono et al., 2001). Thus, three different compressibilities are considered for the px-gt system in the lower mantle, leading to it being either more dense, equally dense or less dense at the CMB than the olivine system. This leads to the density profiles shown in Fig. 2. Note that the shallow (60 km depth) transition in the pyroxene-garnet system leads to the basalt-eclogite transition.

2.3.3. Trace elements

The trace element isotopes ^{235}U, ^{238}U, ^{232}Th, ^{40}K, ^{3}He, ^{4}He, ^{36}Ar and ^{40}Ar are included. As the model does not include continental crust forming processes, it is assumed, following Christensen and Hofmann (1994), that the continental crust has already been extracted, so the initial trace element concentrations listed in Table 4 represent the already depleted man-

Table 4
Isotope concentrations at 3.6 Gyr B.P. and partition coefficients

Symbol	Meaning	Value	Unit[a]	D	Daughter
$[^3He]_0$	Initial ^{3}He	6.12×10^{10}	Atoms/g	0.007	
$[^4He]_0$	Initial ^{4}He	6.00×10^{14}	Atoms/g	0.007	
$[^{238}U]_0$	Initial ^{238}U	9.22×10^{13}	Atoms/g	0.007	^{206}Pb, ^{4}He
$[^{235}U]_0$	Initial ^{235}U	1.34×10^{13}	Atoms/g	0.007	^{207}Pb, ^{4}He
$[^{232}Th]_0$	Initial ^{232}Th	2.48×10^{14}	Atoms/g	0.008	^{208}Pb, ^{4}He
$[^{36}Ar]_0$	Initial ^{36}Ar	1.85×10^{16}	Atoms/g	0.007	
$[^{40}Ar]_0$	Initial ^{40}Ar	2.67×10^{18}	Atoms/g	0.007	
$[^{40}K]_0$	Initial ^{40}K	3.44×10^{15}	Atoms/g	0.01	0.105 ^{40}Ar
$[^{238}U]$	Current ^{238}U	5.28×10^{13}	Atoms/g		
$[^{235}U]$	Current ^{235}U	3.83×10^{11}	Atoms/g		
$[^{40}K]$	Current ^{40}K	4.68×10^{14}	Atoms/g		

[a] To convert from atoms/g to ppb, use the following formula: ppb = (atoms/g) × (atomic weight/Avogadro constant) $\times 10^9$.

tle 3.6 billions years ago after extraction of continental crust. For simplicity, a homogeneous initial composition is assumed for the cases studied here, although this model can also be used to treat a layered initial condition (Tackley and Xie, 2002). Due to radioactive decay, the concentrations of isotopes change continuously with time. The trace elements are partitioned between residue and melt at each melting event, prior to eruption, as in (Christensen and Hofmann, 1994). It is widely believed that most of a magma's noble gas content is outgassed during eruption, but the exact fraction is poorly constrained (e.g., it could be anything between 0.01% and many percent). In the present model, it is assumed that 90% of He and Ar present in erupted material is lost to the atmosphere.

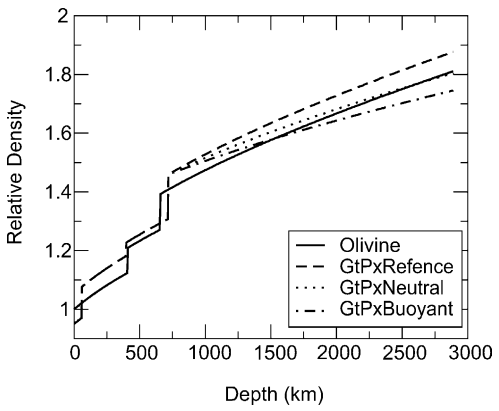

Fig. 2. Density variation along a reference adiabat for the two phase systems. GtPxReference, GtPxNeutral, and GtPxBuoyant are the density profiles with px-gt being more dense, equally dense or less dense at the CMB than the olivine system, respectively.

2.3.4. Radioactive decay processes

Radioactive decay of U, Th and K produces a large part of the heat input in the model (the other is core cooling, as discussed earlier). Thus the internal heating rate varies spatially and temporally according to the local concentration of heat producing isotopes of U, Th and K. Table 3 lists the heat production rate and decay rate of these isotopes. This results in a volume-averaged internal heating rate that falls from ~ 60 to ~ 20 nondimensional units over the course of a calculation, where 1 is 2.7×10^{-13} W/kg.

The radiogenic decays generate noble gases, namely ^{4}He (by decay of U and Th) and ^{40}Ar (by decay of K). After each model time-step Δt the additional amount of radiogenic ingrowth of ^{40}Ar and ^{4}He by U, Th, and K decay in a cell is calculated as follows:

$$\Delta[^{40}\mathrm{Ar}] = 0.105[^{40}\mathrm{K}](1 - \mathrm{e}^{-\lambda_{40}\Delta t}) \tag{15}$$

$$\begin{aligned}\Delta[^4\mathrm{He}] = {} & 8[^{238}\mathrm{U}](1 - \mathrm{e}^{-\lambda_{238}\Delta t}) \\ & + 7[^{235}\mathrm{U}](1 - \mathrm{e}^{-\lambda_{235}\Delta t}) \\ & + 6[^{232}\mathrm{Th}](1 - \mathrm{e}^{-\lambda_{232}\Delta t})\end{aligned} \tag{16}$$

where [ ] indicates concentration at time t, λ_{235}, λ_{238}, λ_{232} are decay constants of ^{235}U, ^{238}U, ^{232}Th, respectively. The constants in Eq. (14) reflect the number of α particles (i.e., ^{4}He) released when ^{235}U, ^{238}U, ^{232}Th

produce ^{207}Pb, ^{206}Pb, ^{208}Pb, respectively. The constant of 0.105 is the fraction of ^{40}K that decays into ^{40}Ar (most ^{40}Ar decays into ^{40}Ca).

2.3.5. Initial concentrations and partition coefficients

Table 4 lists concentrations 3.6 Gyr ago, and current concentrations, for all isotopes considered in the model. It is assumed that at present [U] = 21 ppb, $K/U = 1.27 \times 10^4$, and $Th/U = 3.8$ (Jochum et al., 1983). ^{3}He/^{4}He in primitive meteorites and other extraterrestrial objects is around 200 R_a today (Jeffrey and Anders, 1970; Craig and Lupton, 1981).

The initial ^{3}He and ^{4}He concentrations are calculated such that undifferentiated, undegassed material would have ^{3}He/^{4}He $= 35R_a$, similar to the Loihi source, which is consistent with Loihi samples having a primitive origin. This leads to ^{3}He/^{4}He $= 180R_a$ at $t = 4.5$ Gyr ago. Note that in undifferentiated, undegassed material the concentration of ^{3}He does not change whereas the concentration of ^{4}He increases due to ^{4}He ingrowth from U and Th decay. The calculated initial concentration of ^{3}He at 4.5 Gyr ago is consistent with other estimates (e.g. Harper and Jacobsen, 1996).

The partition coefficients of noble gases between melt and solid are rather uncertain but some experimental measurements exist. Possible ranges of coefficients are: $K_{He} \leq 0.07$ and $K_{Ar} = 0.05$–0.15 (Hiyagon and Ozima, 1986). The distribution coefficients of noble gases are insensitive to, or even positively correlated with the atomic size of noble gases. Thus, the relative compatibility of helium and uranium is still unknown, but it has a large effect on the evolution of isotope ratios. If He is more compatible than U and Th then the residue from melting develops a high ^{3}He/^{4}He signature (e.g. Graham et al., 1990). It may also be possible for residue to develop a high ^{3}He/^{4}He signature relative to mean mantle even if He is less compatible, if the mean mantle loses He through outgassing fast enough (Coltice and Ricard, 2002). Thus to test these possibilities three values for the partition coefficient for helium are tried: equally compatible, 10 times more compatible, or 10 times less compatible than U. The partition coefficient for uranium is fixed at $D = 0.007$ for all cases (Hofmann, 1988). The argon partition coefficient is assumed to be the same as for helium in all cases. Table 4 lists the elemental partition coefficients for all isotopes.

3. Results

3.1. Cases

Five Earth-like cases are presented here: a reference case, in which the partition coefficient for He is the same as that for U and Th and the crustal component is dense at the CMB, two cases with different He partition coefficients (10 times more compatible and 10 times less compatible), and two cases with differing compositional buoyancy in the deep mantle (crust is either equal in density to the other component or less dense, as in Fig. 2). Compositional density variations down to 720 km are identical in all cases. Cases are run for the last 3.6 billion years of Earth history, with some cases also run for 4.5 billion years.

Three cases are presented for each of Venus and Mars. All cases have analogous physical properties to the Earth reference case except for the lack of lithospheric yielding as discussed earlier, but vary in reference *Ra* (equivalent to varying reference viscosity). All cases are run for 4.5 billion years.

Temperature is initialized to an adiabat with potential temperature 1800 K, with error function thermal boundary layers of nondimensional thickness 0.03 at top and bottom, and small (peak-to-peak amplitude 0.01) random perturbations. Care was taken to choose the initial adiabat so that the temperature profile was everywhere lower than the solidus, to avoid a huge pulse of melting in the first time-step. The initial CMB temperature is 4065 K, which includes 500 K of 'superheat' relative to the CMB temperature corresponding to the 2500 K superadiabatic temperature scale listed in Table 1.

3.2. Interior structure

In the reference case, the compositional field (Fig. 3d) indicates that a thick layer of dense, subducted oceanic crust has built up at the base of the mantle, with a thin crust near the surface. A layer of depleted residuum has also built up below the '660' phase boundary, probably due to the anomalous compositional buoyancies existing in the 660–720 km depth interval due to the differing depths of the olivine-system and pyroxene-garnet system phase transitions. The dense, recycled crustal layer above the CMB is enriched in heat producing incompatible

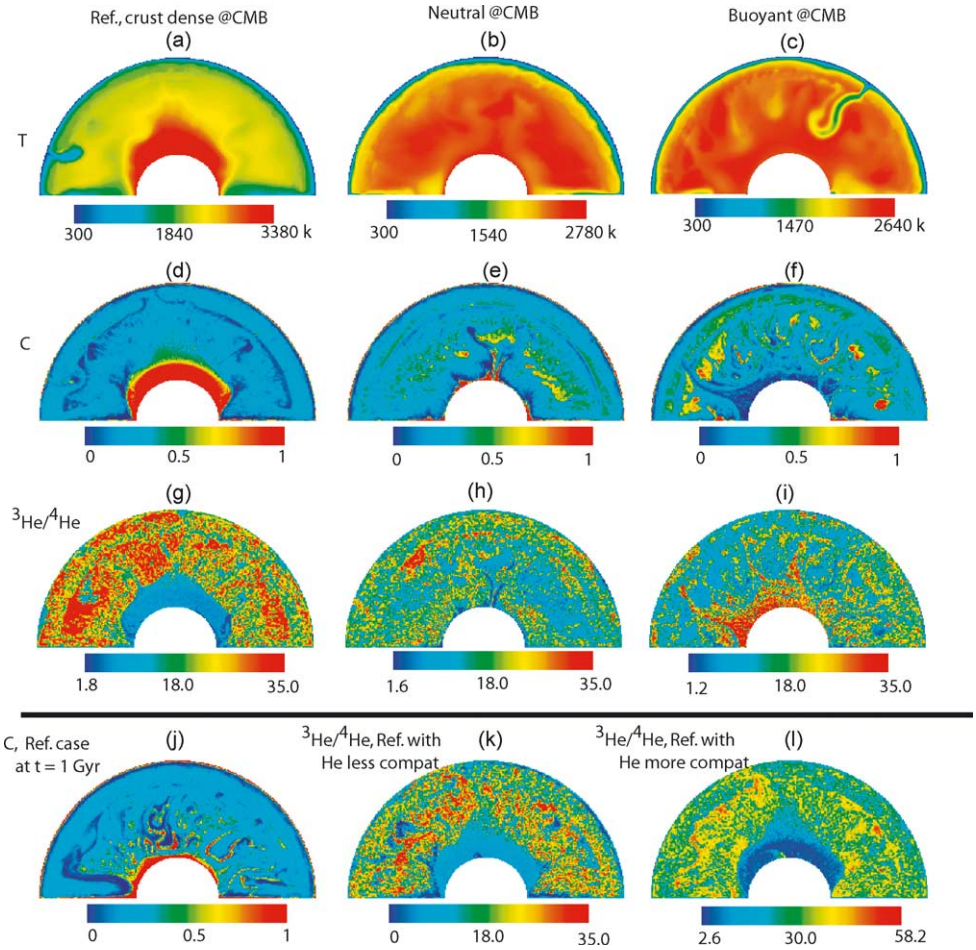

Fig. 3. Earth internal structures at present day (after 3.6 Gyr except (j)) of reference case (left column), case with neutral buoyant crust at CMB (middle column, except k), case with buoyant crust at CMB (right column, except l), case with helium less compatible than uranium (k), case with helium more compatible than uranium (l). (a–c) Temperature field, from cold (blue) to hot (red). (d–f) Composition, ranging from basalt/eclogite (red) to harzburgite (blue). (g–l) except (j) $^{3}He/^{4}He$ (relative to atmospheric value) ranging from min (blue) to max (red). (j) Composition field of reference case at $t = 1.0$ Gyr.

elements ^{40}K, U and Th because they partition into the crust on melting. The resulting intense heat production causes the layer to get almost as hot as the core-mantle boundary (CMB), as seen in the temperature field (Fig. 3a). This hot layer is not formed immediately, but continuously with time (see Fig. 3j for a composition field snapshot at $t = 1.0$ Gyr).

The case with crust that is neutrally buoyant at the CMB (Fig. 3e) displays only a transient crustal layer at the CMB, with some compositional stratification around 660 km as indicated by a residue-enriched region below 660 km depth and a crust-enriched region in the transition zone. In the case with crust that is buoyant at the CMB (Fig. 3f), a layer of residue accumulates above the CMB, and blobs of crustal material accumulate in the mid-lower mantle where they are neutrally buoyant. The transition zone is also enriched in the crustal component. Unlike the reference case, these two cases do not have a hot basal layer (Fig. 3b and c).

Cases with differing Helium partition coefficients have the same compositional and temperature fields (which are therefore not illustrated) but differ greatly in the spatial distribution of the $^{3}He/^{4}He$ ratio. How-

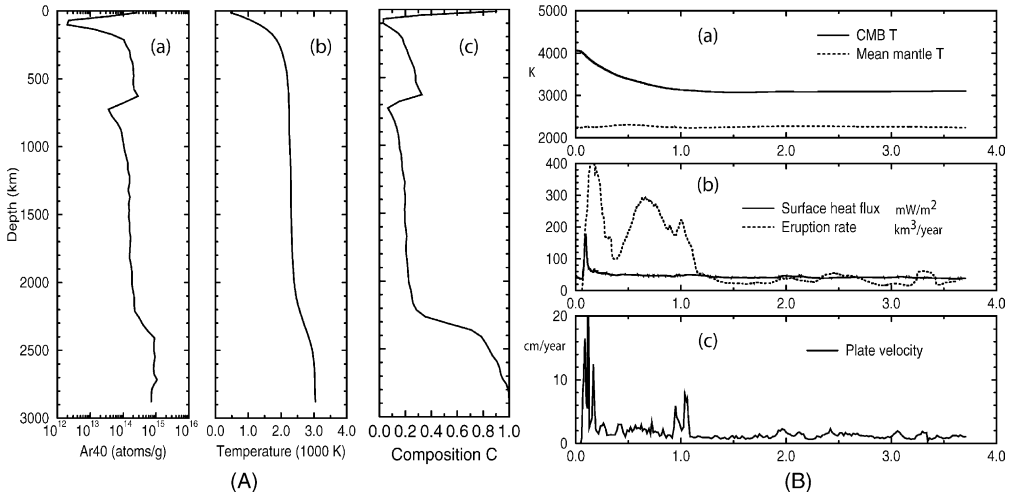

Fig. 4. (A) Profiles of horizontally-averaged quantities for reference case: (a) Ar^{40}. (b) Temperature. (c) Composition. (B) Time evolution of the reference case. (a) Mean mantle temperature and CMB temperature. (b) Surface heat flux and eruption rate. (c) Plate velocity.

ever, $^3He/^4He$ is always low in recycled crust because the crust is largely degassed while at the same time enriched in U and Th, which produce ^4He.

When He is less compatible than U, $^3He/^4He$ (Fig. 3k) is highest in material that has never participated in melting. For the opposite case (He is more compatible than U), $^3He/^4He$ (Fig. 3l) is highest in recycled residuum, because the concentrations of U and Th, which produce ^4He, are depleted by a greater factor than the concentration of ^3He, so $^3He/^4He$ decreases with time less rapidly than it does in primitive, unmelted material. If He and U have the same compatibility (Fig. 3g), the resulting $^3He/^4He$ distribution is a combination of the above two cases. In the case with crust buoyant at the CMB (Fig. 3i), it is notable that $^3He/^4He$ is high in the residuum layer at the base. If plumes rise from this layer then they could form OIB with high $^3He/^4He$, although this layer would not explain the enriched refractory components (e.g., HIMU).

Depth profiles of present-day horizontally-averaged argon concentration, temperature, and composition are shown in Fig. 4. The composition profile clearly shows the crustal layers at the top and bottom, and the localized stratification around 660 km depth induced by the composition-dependent phase transitions. The geotherm shows the warming up of the dense crustal layer and the lack of a thermal boundary layer at the CMB. The ^{40}Ar concentration is high in the deep crustal layer because this layer is enriched in ^{40}K, and depleted in the lithosphere due to partial melting. In the "MORB source region" below the lithosphere, the ^{40}Ar concentration is about five times lower than in the deep layer, which is qualitatively consistent with the "missing argon" paradox discussed earlier: a large fraction of the remaining argon could be stored in a deeper layer.

3.3. Outgassing and time evolution

The time evolution of reference case mantle and CMB temperatures, heat flux, eruption rate, and surface (plate) velocity (Fig. 4) indicate an early, ~1 Gyr long phase of rapid eruption, plate motion and core cooling, after which activity seems to remain roughly constant with time. This early phase of abundant magmatism followed by a slower phase persisting to the present day was found in all model runs. Interestingly, this time evolution does not appear to follow the simple scaling laws followed by simple convection systems (e.g. Honda et al., 1993) and used in parameterized convection modeling. This difference is due to the interplay of complexities such as ongoing compositional stratification (e.g. Nakagawa and Tackley, 2003), yielding-induced plate behavior, and phase transitions, and must be further anayzed in the future.

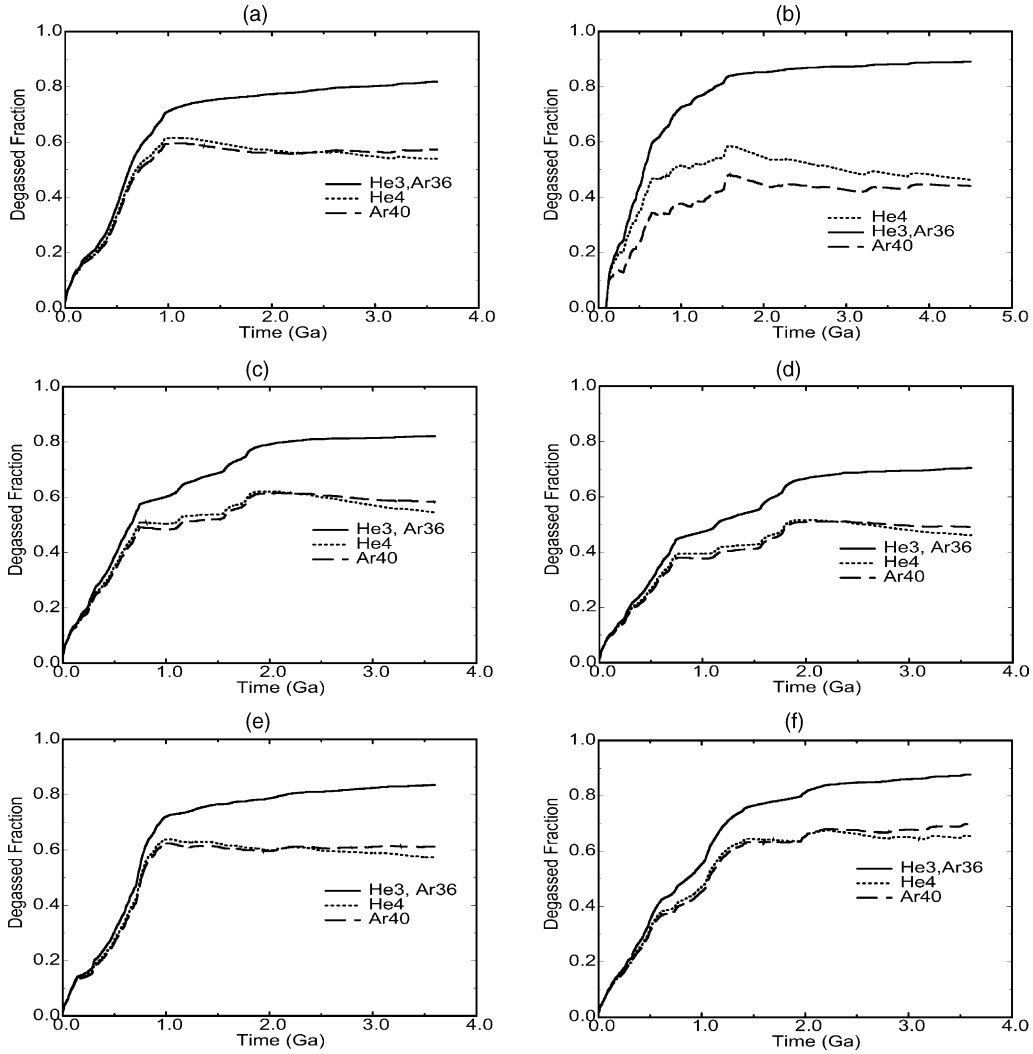

Fig. 5. Outgassing of He and Ar isotopes vs. time, expressed as a fraction of the total amount of each isotope (which increases with time for ^{4}He and ^{40}Ar). (a) Reference case starting 3.6 Gyr ago. (b) Reference case starting 4.5 Gyr ago. (c) Helium is less compatible than uranium. (d) Helium is more compatible than uranium. (e) Crust neutral at CMB. (f) Crust buoyant at CMB.

Eruption of magma is the key mechanism for releasing mantle noble gases to the atmosphere, since diffusion through the solid crust or lithosphere is probably too slow. The presented models degas around 50–60% of radiogenic ^{40}Ar, consistent with common estimates, and about 80–90% of non-radiogenic species such as ^{3}He and ^{36}Ar (Fig. 5), indicating that more than 90% of ancient material has been processed through partial melting, consistent with other convection calculations (e.g. Davies, 2002). The curves for ^{3}He and ^{36}Ar are identical because they have the same model partition coefficients and they participate in the same melt fractionation and degassing processes. The outgassed fraction of radiogenic daughter isotopes ^{4}He and ^{40}Ar may decrease with time if radiogenic ingrowth occurs faster than outgassing.

All models show rapid outgassing early on, with more gradual outgassing after about 1 Gyr. To first order this is expected even for a simple, single-reservoir model with constant eruption rate, which would pro-

duce a (1-exp) time-dependence (Albaredè, 2003), but, as discussed earlier, the present cases also undergo a change in convective style with associated reduction in magmatic rate. Outgassed fractions are in the same range if the models start 4.5 Gyr ago (Fig. 5b) instead of 3.6 Gyr ago. The reason for this is that the early phase of vigorous activity lasts approximately the same length of time regardless of how far in the past the run is started. This implies that, while the slowing down is caused partly by the decay of heat producing elements and secular cooling of the mantle and core, the chemical stratification of the mantle that results from differentiation plays a major role in imposing a self-limiting behavior on the rate of activity, and may help to explain why there is little difference between running the models for 3.6 and 4.5 Gyrs.

Outgassing efficiency is observed to slightly depend on partition coefficients and crustal density. When helium is more compatible (Fig. 5d), more helium and argon are retained in the residuum, therefore, the degassing efficiency is lower than that in Fig. 5(c) where helium and argon are less compatible. Regarding the effect of crustal density on degassing efficiency, less outgassing is observed when the crust is denser in the deep mantle, because segregated material rich in radiogenic gases prevents degassing of ^{4}He and ^{40}Ar.

In order to be applicable to understanding the real Earth, it is important that the rate of differentiation, as indicated by the rate of crustal production, be of similar magnitude to Earth's. Unfortunately the only firm information for Earth pertains to the present day and recent past. The model eruption rate for the reference case averaged over the last 100 Myr is 29.6 km^3/year (Fig. 4(A)(b)), ∼1.5 times the present-day oceanic crustal production rate of 21 km^3/year (Stacey, 1992). This model eruption rate was scaled from cylindrical geometry to Earth's spherical geometry based on the volume ratios of the two domains, which recognizes that the geochemically-important rate is (fraction of the mantle)/(time nterval). This eruption rate is accomplished by a convective vigor that is, at the end of the simulations ("present day"), indicated by the surface heat flux of 47.1 mW/m^2 and an rms. surface velocity of 1.2 cm/year (Fig. 4 (A)), which are factors of ∼1.7 and ∼3.2 lower than Earth's, respectively, implying that the effective Rayleigh number is about five times too low. Despite the lower surface velocity, the crustal production rate is in Earth's range because the oceanic crustal thickness is about three times higher than Earth's (as in the previous study of (Christensen and Hofmann, 1994)), which occurs because mantle temperature is higher and because melting occurs over a wider horizontal region than at real mid-ocean ridges.

3.4. Helium ratio distributions

Helium ratio histograms for the five cases are plotted in Fig. 6 for comparison with the observations (Fig. 1). The histograms are calculated in three different ways: (i) for the whole mantle counting each tracer as one sample, (ii) for the whole mantle, using each grid cell as one sample, which therefore involves summing abundances over all tracers in a cell before taking the average, and (iii) for erupted material during the last ∼ 150 Myr of the simulation.

The effect of He partitioning on whole mantle ^{3}He/^{4}He distributions is shown in the top three plots in the left column (Fig. 6a, d and g). With He less compatible (Fig. 6a), the small peak at a ratio of 35 R_a is caused by the few percent of remaining undifferentiated 'primitive' material. The peak at very low values is associated with crustal material, and the in-between values are associated with residue of various ages. These in-between values may be consistent with the models of (Coltice and Ricard, 1999; Ferrachat and Ricard, 2001), in which residuum may have a higher ^{3}He/^{4}He than the mantle average, if the average mantle becomes degassed such that its ^{3}He/^{4}He ratio falls faster than that of ancient residuum. However, in these calculations any remaining unmelted material has higher still ^{3}He/^{4}He. With equal He compatibility (Fig. 6d), the peak at 35 R_a corresponds to both unmelted material and depleted residue, while the other values are for crust of varying age. With He more compatible (Fig. 6g), ratios greater than primitive can be developed as indicated by the spectrum of values extending up to 74 R_a, which is associated with residue. Unmelted material causes the peak at 35 R_a. Crustal density in the deep mantle does not affect the location of the peaks in these whole mantle distributions (Fig. 6j, and m).

Different sampling methods can give dramatically different ^{3}He/^{4}He distributions. The effect of cell sampling (middle columns) rather than tracer sampling is to greatly smooth the distributions, but it may also move or obscure the peaks, as shown in Fig. 6a and b,

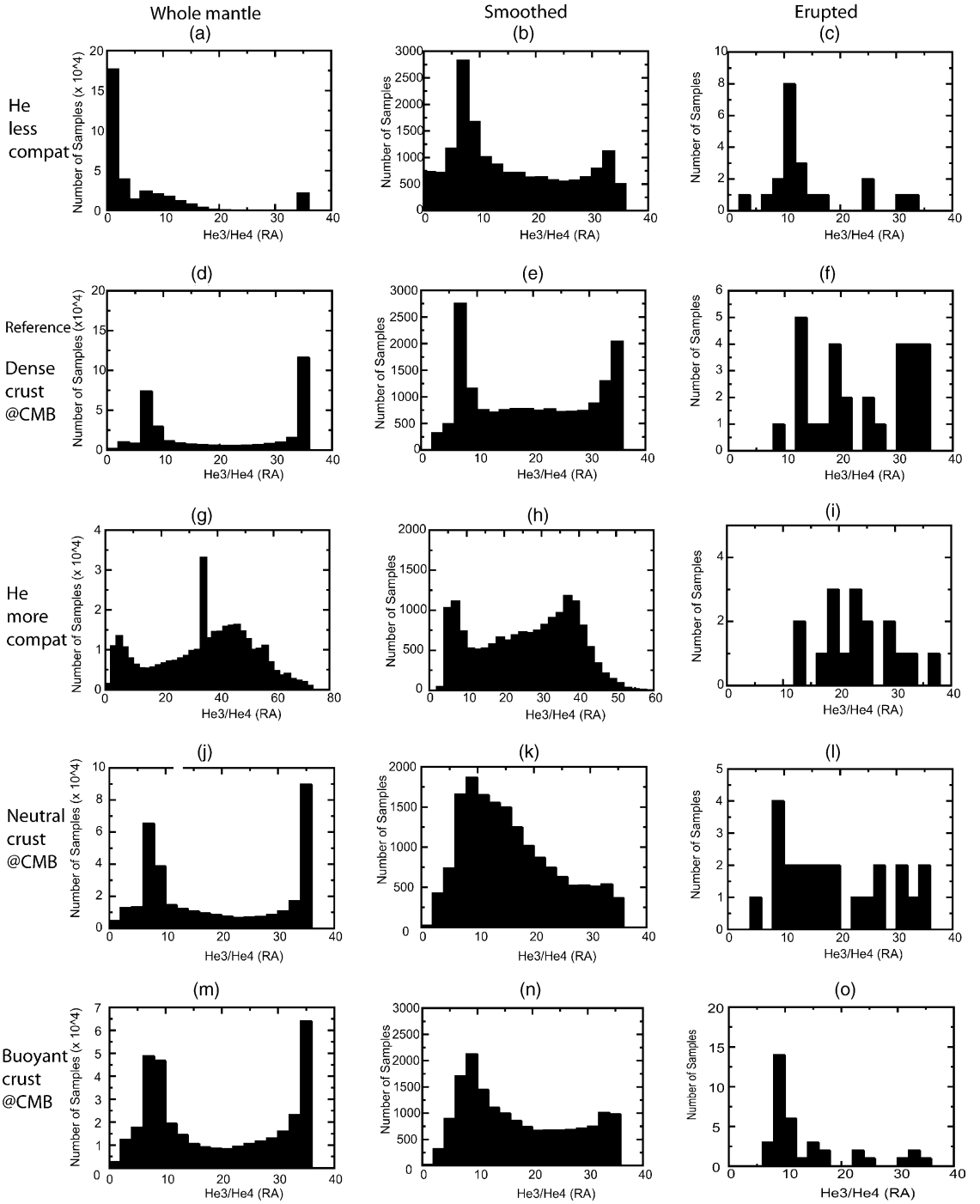

Fig. 6. Effect of helium partitioning, crustal density, and sampling method on present-day (after 3.6 Gyr integration) $^3He/^4He$ distribution. Left column, tracer-based sampling. Middle column, cell-based sampling (with 256×64 sampling cells, corresponding to $35\,km \times 45\,km$ average sampling size). Right column, surface eruption sampling. (a–c) Helium less compatible than uranium. (d–f) Reference case. (g–i) Helium more compatible than uranium. (j–l) crust neutral at CMB. (m–o) crust buoyant at CMB.

where the lower peak has moved from close to zero to 7 R_a, or Fig. 6j and k where the lower peak has been greatly smeared out and the upper peak lost. When summing isotope abundances over cells, tracers that are more depleted in He have less influence on the ratio, so the distribution is skewed towards components that have higher He concentrations. Note that, as in (Christensen and Hofmann, 1994), tracers carry amounts of trace elements so calculating cell isotope ratios simply involves summing these amounts prior to taking the ratio.

The distribution that is sampled by surface magmatism may be quite different from either mantle-averaged distribution, because of chemical stratification. Melting also causes a local averaging of isotope ratios, so the most useful comparison is with the cell-averaged distributions. Two cases display a rather Earth-like (i.e., MORB-like) surface-sampled distribution of He ratios, with a peak at $\sim 10 R_a$ and scatter either side of this: the "He less compatible" case (Fig. 6 c) and the "Buoyant crust" case (Fig. 6o). Other cases lack a strong peak at the MORB value and are dominated by scattered higher values. The success of these two cases can be understood in terms of the chemical stratification discussed earlier. In the reference case (Fig. 6f), the shallow mantle is dominated by depleted material which, due to equal He and U compatibility, has high ^{3}He/^{4}He. Lower compatibility of He relative to U (Fig. 6c) gives this depleted material lower ^{3}He/^{4}He, in this case similar to the MORB source. Alternatively, recycled crust has very low ^{3}He/^{4}He and a high ^{4}He concentration and when its deep mantle density prevents it from settling into a layer (Fig. 6o), it mixes back into the upper mantle in sufficient abundance to decrease ^{3}He/^{4}He to a MORB-like value.

3.5. Interior structures and outgassing on Venus and Mars

In Venus and Mars, the lack of plate tectonics makes heat transport less efficient, causing the interior to heat up (Fig. 7), which might produce more melt, other things being equal. However, this is mitigated by the pervasive thickness of the lithosphere, i.e., there are no spreading centers where mantle can adiabatically upwell to very shallow depths and produce melt. In the present results, these effects seem to balance, such that the total amount of melting, and the fraction of noble gases that are outgassed, are in the same range as Earth's.

3.5.1. Venus

Here, results are compared for three different reference Rayleigh numbers, corresponding to three different reference viscosities. Fig. 7(A) composition fields indicate that although plate tectonics is lacking on Venus, some crustal material delaminates, perhaps assisted by negative buoyancy caused by the basalt to eclogite transformation, and is stored either in the mantle transition zone (Fig. 7(A)b) or at core mantle boundary (Fig. 7(A)e and h). The transition zone enforces a larger layering effect at lower *Ra* than it does at higher *Ra*. This surprising result appears to come from the interaction between compositional variations and the phase transition, which here dominates the previously-studied interaction between thermal up/downwellings and the phase transition (Christensen and Yuen, 1985). The ^{36}Ar distributions (Fig. 7(A) c, f and i) show the locations of undegassed (high ^{36}Ar) and degassed (low ^{36}Ar) material. The crust is not of uniform thickness but appears to be thickened in some areas, suggesting that some lid deformation still occurs despite the large viscosity contrast, which is not as large as the actual viscosity contrast in Venus (Solomatov and Moresi, 1996). Indeed, the model Venus is not in a pure stagnant lid state; rather, the surface is deforming and moving, causing episodic melting in some cases (e.g., Fig. 8(c)). This is perhaps consistent with latest observations that Venus may periodically resurface itself completely through volcanic eruptions.

Outgassing can be compared to the estimate of Kaula (1999). He estimated that about 24(±10)% of the radiogenic ^{40}Ar produced in the mantle since Venus's formation has been outgassed, compared to ∼50% for Earth, the lower efficiency of Venus being attributed to its lack of plate tectonics and relatively sluggish convection caused by higher mantle viscosity due to dryness. Fig. 8 left column indicates that higher Rayleigh number results in greater outgassing, with the two higher Rayleigh number cases (Fig. 8c and e) outgassing as much as the Earth-like cases. To match the 24% degassing efficiency estimated by Kaula (1999), the reference Rayleigh number has to be as low as 10^6 (Fig. 8a), corresponding to a reference mantle viscosity of 10^{23} Pa s. In this case,

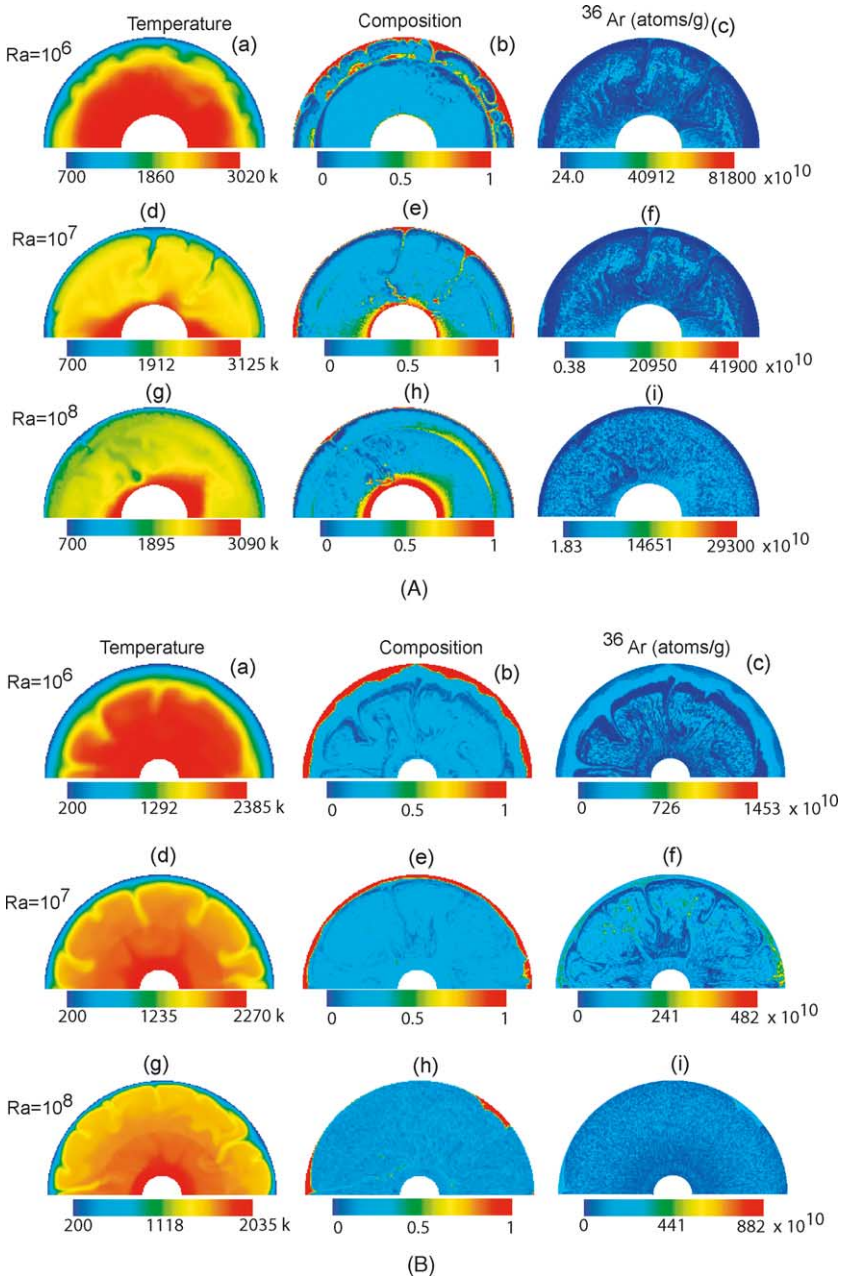

Fig. 7. (A) Interior structure of Venus-like planet after 4.5 Gyr. (a), (d), (g) Temperature field, from low (blue) to high (red). (b), (e), (h) Composition field, from harzburgite (blue) to basalt (red). (c), (f), (i) ^{36}Ar concentration, from low (blue) to high (red). (B) Interior structure of Mars-like planet after 4.5 Gyr. Caption is the same as in (A).

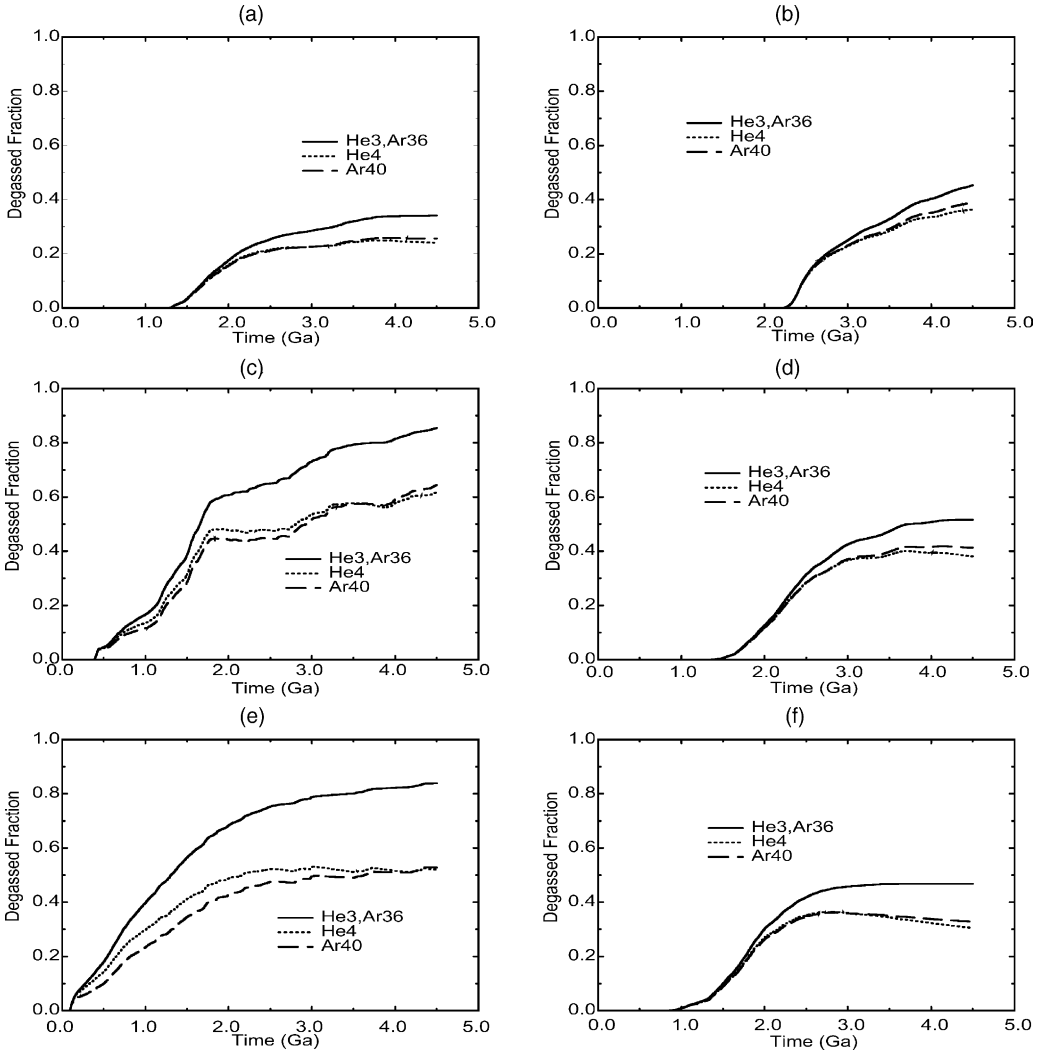

Fig. 8. (Left column) Degassing history of Venus-like planet. (Right column) Degassing history of Mars-like planet. (a),(b) $Ra = 1.0 \times 10^6$. (c), (d) $Ra = 1.0 \times 10^7$. (e), (f) $Ra = 1.0 \times 10^8$.

only about 25% of ^{40}Ar has been degassed, and other species like ^{36}Ar (Fig. 8(A)c) are less depleted than in other two cases (Fig. 7(A) f and i). Note that there is a delayed onset of outgassing that is greater for lower reference Rayleigh numbers. This is because it takes time for the interior to heat up sufficiently to produce melt at depths below the relatively thick lithosphere, as found previously by Reese et al. (1999). Lower reference *Ra* (higher reference viscosity) results in a thicker lithosphere, so that more heating up is required to reach the sub-lithospheric solidus (Fig. 7(A)a, d, and g). This could be compensated for by starting the lower *Ra* runs from a hotter initial state, but for these initial calculations it was thought best to start from identical initial states.

In these models an end-member scenario is assumed: that all melt produced in the mantle erupts at the surface to form crust. With this assumption, outgassing fractions that are similar to Earth's can be obtained despite the lack of plate tectonics. However, it seems likely that instead, a substantial fraction of the produced melt would not migrate all the way to

the surface and erupt, in which case the amount of outgassing would be substantially lower, perhaps consistent wih the estimate of Kaula (1999). As discussed above a high mantle viscosity (Fig. 8a) also reduces outgassing and is within the range of uncertainties. In conclusion, Kaula (1999)'s estimate for radiogenic Ar outgassing seems reasonable from these numerical models and could be satisfied by high mantle viscosity or inefficient melt escape, or a combination of these.

3.5.2. Mars

The three Mars cases look more similar to conventional rigid lid convection than the Venus cases, with no obvious settling of recycled crust (Fig. 7(B)a–e, g and h), indicating that any delaminated crust simply mixed efficiently, particularly at higher Ra. The depth of the basalt to eclogite phase transition is much greater on Mars due to lower gravity, so this would not play as large a role in destabilizing crust. The most likely parameter range (*Ra*) for Mars (Table 1) lies at the low end of the investigated range. Again, the onset of magmatism is increasingly delayed as *Ra* is decreased due to the longer time required to heat up sufficiently to melt material below the base of the lithosphere. Although in a rigid lid state, the model melts and degasses continuously due to the hot interior. These sublithospheric hot materials may cause long-lived large scale volcanism on Mars (Schott et al., 2001). Curiously, ^{36}Ar concentration is reasonably high in the crust (Fig. 7(B)c, f, and i) because ^{36}Ar is concentrated in melt due to its incompatibility, and only outgassed by 90% in these calculations.

These numerical models predict a higher outgassing efficiency than that estimated from the current Martian atmosphere ^{40}Ar concentration, which can be used to estimate what fraction of these species have been lost to space. The presented models indicate that about 30–40% of radiogenic argon has outgassed over the past 4.5 Gyr (Fig. 8 right column), regardless of reference viscosity (Rayleigh number). Based on this, it is estimated that more than 90% of the outgassed argon has been lost to space due to the impact of O^+ ions pick up and solar wind (Jakosky and Jones, 1997). The present results support the model of Hutchins and Jakosky (1996). Loss of noble gases and other species is thus an important factor that must be addressed in studying Martian atmosphere evolution.

4. Discussion and conclusions

4.1. Outgassing on Mars and Venus

It seems that Kaula (1999)'s estimate of 24(±10)% radiogenic argon outgassing on Venus is dynamically reasonable, and may be matched either by Venus having a much higher mantle viscosity than Earth, i.e., of the order of 10^{23} Pa s, or by incomplete (e.g., ∼50%) eruption (outgassing) of produced melt. For Mars, a comparison between model and observations is much more difficult, but it appears difficult to avoid ∼30–40% outgassing, implying that Mars must have lost most of its atmospheric noble gases to space.

A successful model must match not only time-integrated constraints such as total outgassing, but also constraints on the time-dependence of magmatic history. On Venus, there is believed to be ongoing volcanic activity, with some researchers even preferring a continuous resurfacing model to the popular catastrophic resurfacing one (different models are summarized, in e.g. Namiki and Solomon, 1998), so any of our Venus models would be within the range of proposed hypotheses. Mars is probably volcanically dead, although there has been long-lived large-scale volcanism (Schott et al., 2001) and possibly some relatively young (∼100 s Ma) lava flows from Olympus Mons. The presented $Ra = 10^7$ or $Ra = 10^8$ models would be consistent with that history (based on the gradients of the curves in Fig. 8).

It has commonly been proposed that Venus' mantle has a higher viscosity than Earth's, and this has generally been attributed to a lack of water in Venus' mantle, which could increase the viscosity by at least two orders of magnitude under identical conditions (e.g., temperature) (Hirth and Kohlstedt, 1996). However, this would be partially compensated by the heating up of Venus' mantle; the increased temperature would diminish the viscosity. Nevertheless, higher mantle viscosity is also supported by other considerations, particularly the strong positive correlation between topography and geoid on Venus. For example, modeling of the geoid and topography of broad highland regions indicates that if these features are plume-related, then the mantle of Venus can not have an Earth-like low viscosity zone in its upper mantle (Kiefer and Hager, 1991).

4.2. Noble gases within Earth's mantle

The presented thermo-chemical models simultaneously match the constraint on total ^{40}Ar outgassing, self-consistently evolve regions that have the range of ^{3}He/^{4}He ratios observed in oceanic basalts, and (in some cases) obtain MORB-like ^{3}He/^{4}He distributions in erupted material, all from a chemically homogeneous initial state. The models also develop considerable chemical stratification as a result of the relative buoyancies of differentiated components (crust and residue). Non-radiogenic species are outgassed by $\sim$ 90%, which indicates that more than 90% of the mantle has been processed through melt extraction. These results suggest that layered convection is not necessary to obtain the observed signatures for He and Ar. Furthermore, Ar is depleted in the model MORB source region relative to the mantle average due to segregation of K in the deep mantle, which is qualitatively consistent with the "missing argon" paradox (Allègre et al., 1996; Ballentine et al., 2002), although this must be quantified in future.

High ^{3}He/^{4}He is obtained in the model whether helium is more compatible or less compatible than U, but through different mechanisms. If less compatible then the high ratios are associated with unmelted material; if equally compatible then they are associated with either unmelted or residuum material, and if more compatible then the highest ratios are associated with recycled residue. Coltice and Ricard (1999), Coltice et al. (2000b), Ferrachat and Ricard (2001) proposed a model in which residue may contain the highest ^{3}He/^{4}He even if He is less compatible than U, if the average mantle is outgassing at a fast enough rate. The presented case in which He is less compatible indeed shows that residue can have high ^{3}He/^{4}He relative to the average, but that undifferentiated material has the highest ^{3}He/^{4}He.

Deep mantle crustal density strongly influences the ^{3}He/^{4}He distribution sampled magmatically, because it affects the ability of subducted crust, which is depleted in gases but strongly enriched in U and Th, to mix back into the MORB source region. If crust is relatively dense at the CMB then it segregates into a layer, resulting in a strongly depleted shallow mantle, whereas if neutral or buoyant, it mixes back into the rest of the mantle, decreasing ^{3}He/^{4}He. Due to multi-component phase transitions, recycled crust has a tendency to build up in the transition zone, and (if buoyant at the CMB) in a zone of neutral buoyancy in the mid- lower mantle, while depleted residuum builds up below the transition zone.

The calculated ^{3}He/^{4}He histogram depends strongly on the method of sampling due to two effects: averaging and chemical stratification. Histograms calculated using each tracer as a sample are different from those in which abundances are first integrated over each grid cell. Most importantly, the ^{3}He/^{4}He distribution histogram for erupted material may be quite different from the mantle-wide average, because it preferentially samples the shallow mantle.

Two cases generate "Earth-like" (i.e., MORB-like) distributions of ^{3}He/^{4}He in surface magmatism. In one of these, the shallow mantle is depleted due to recycled crust settling into a layer at the bottom, and He is less compatible than U, which brings the ^{3}He/^{4}He ratio in residue down to MORB-like values. In the other, He is equally compatible to U but recycled crust mixes back into the shallow mantle causing sufficient ingrowth of radiogenic ^{4}He to lower ^{3}He/^{4}He. Most probably a spectrum of successful solutions exists with a trade-off between He compatibility and deep mantle crustal density, so this non-uniqueness needs to be further explored in future calculations. Improved knowledge of key physical parameters, particularly the partition coefficient for He and the deep-mantle density of eclogite, would narrow this ambiguity.

All cases display lateral chemical heterogeneity at all lengthscales, regardless of whether settling of crust or residue takes place. This is consistent with the old "marble cake" concept of mantle heterogeneity (Allègre and Turcotte, 1986), versions of which have been proposed in various recent studies that attempt to explain chemical observations and were discussed in the Introduction (Coltice and Ricard, 2002; Helffrich, 2002; Meibom et al., 2003; Meibom and Anderson, 2003). Thus, a mantle that is highly heterogeneous, as well as vertically stratified, appears likely from these modeling results as well as other considerations.

4.3. Model limitations and future directions

While the results are very promising, there are several limitations in the model, which should

be addressed in future studies. Some major ones are:

(1) The presented calculations are in 2D, due to the computational expense of the tracer-based compositional treatment. In 3D, stirring and mixing may be less (Schmalzl et al., 1996) or more (Ferrachat and Ricard, 1998) efficient, and it should be possible to distinguish plume-related melting and therefore compute separate signatures for model OIB and MORB.
(2) The model convective regime is not Earth-like in two respects. Firstly the convective vigor is less than Earth-like, which may make mixing and re-homogenization of differentiated components less efficient than it is in the real Earth. Secondly, the thicker-than-Earth-like oceanic crust (which compensates for the reduced plate velocity) may indicate a larger total fraction of melting at spreading centers than the 8–10% commonly believed, which would reduce the concentration of incompatible elements in the crust and subsequent deep segregated layer accordingly, affecting mass balance calculations.
(3) A successful model must simultaneously reconcile constraints from all the isotope systems, not just noble gases and their parents. The authors are actively working on modeling the evolution of systems such as Pb isotopes and Nd-Sm, and this will be reported in a future paper.
(4) Continental crust is thought to play a major role in the evolution of geochemical signatures (e.g. Coltice et al., 2000a), so the continuous formation and recycling of continents must somehow be incorporated in the future. Continents also have a first-order effect on large-scale mantle flow and dynamics (e.g. Zhong and Gurnis, 1993).

Acknowledgements

This research was supported by Los Alamos National Laboratory, the David and Lucile Packard Foundation, NSF grant EAR0207741 and NASA grant NAG 5-3956. Reviews by P.E. van Keken, N. Coltice and two anonymous reviewers were very helpful in improving this manuscript, as were comments by Francis Albarède.

References

Albarède, F., 1998. Time-dependent models of U-Th-He and K-Ar evolution and the layering of mantle convection. Chem. Geol. 145, 413–429.
Albarède, F., 2003. Geochemistry. Cambridge University Press, Cambridge, 248 pp.
Allègre, C.J., Hofmann, A., O'Nions, K., 1996. The Argon constraints on mantle structure. Geophys. Res. Lett. 23, 3555–3557.
Allègre, C.J., Moreira, M., Staudacher, T., 1995. $^{4}He/^{3}He$ dispersion and mantle convection. Geophys. Res. Lett. 22, 2325–2328.
Allègre, C.J., Staudacher, T., Sarda, P., Kurz, M., 1983. Constraints on evolution of Earth's mantle from rare gas systematics. Nature 303, 762–766.
Allègre, C.J., Turcotte, D.L., 1986. Implications of a two-component marble-cake mantle. Nature 323, 123–127.
Anderson, D.L., 1993. Helium-3 from the mantle: primordial signal or cosmic dust. Science 261 (5118), 170–176.
Anderson, D.L., 1998. A model to explain the various paradoxes associated with mantle noble gas geochemistry. Proc. Natl. Acad. Sci. USA 95 (16), 9087–9092.
Ballentine, C.J., van Keken, P.E., Porcelli, D., Hauri, E.H., 2002. Numerical models, geochemistry and the zero-paradox noble-gas mantle. Phil. Trans. R. Soc. Lond. A 360, 2611–2631.
Burnard, P.G., Farley, K.A., Turner, G., 1998. Multiple fluid pulses in a samoan harzburgite. Chem. Geol. 147, 99–114.
Christensen, U.R., Hofmann, A.W., 1994. Segregation of subducted oceanic crust in the convecting mantle. J. Geophys. Res 99 (B10), 19867–19884.
Christensen, U.R., Yuen, D.A., 1985. Layered convection induced by phase transitions. J. Geophys. Res 90 (B12), 10291–10300.
Coltice, N., Albarè, F., Gillet, P., 2000a. ^{40}K-^{40}Ar constraints on recycling continental crust into the mantle. Science 288, 845–847.
Coltice, N., Ferrachat, S., Ricard, Y., 2000b. Box modeling the chemical evolution of geophysical systems: case study of the Earth's mantle. Geophys. Res. Lett. 27, 1579–1582.
Coltice, N., Ricard, Y., 1999. Geochemical observations and one layer mantle convection. Earth Planet. Sci. Lett. 174, 125–137.
Coltice, N., Ricard, Y., 2002. On the origin of noble gases in mantle plumes. Phil. Trans. R. Soc. Lond. A 360, 2633–2648.
Craig, H., Lupton, J.E., 1981. Helium-3 and mantle volatiles in the ocean and the oceanic crust. In: Emiliani, C. (Ed.), The Sea: The Oceanic Lithosphere, vol. 7. Wiley, New York, pp. 391–428.
Davies, G.F., 1999. Geophysically constrained mantle mass flows and the ^{40}Ar budget: a degassed lower mantle? Earth Planet. Sci. Lett. 166, 149–162.
Davies, G.F., 2002. Stirring geochemistry in mantle convection models with stiff plates and slabs. Geochem. Cosmochem. Acta 66, 3125–3142.
Farley, K.A., Natland, J.H., Craig, H., 1992. Binary mixing of enriched and undegassed (primitive?) mantle components (He, Sr, Nd, Pb) in Samoan lavas. Earth Planet. Sci. Lett. 111, 183–199.
Farley, K.A., Neroda, E., 1998. Noble gases in the Earth's mantle. Annu. Rev. Earth Planet. Sci. 26, 189–218.

Ferrachat, S., Ricard, Y., 1998. Regular vs. chaotic mantle mixing. Earth Planet. Sci. Lett. 155, 75–86.

Ferrachat, S., Ricard, Y., 2001. Mixing properties in the Earth's mantle: effects of the viscosity stratification and of oceanic crust segregation. Geochem. Geophys. Geosyst. (2) Paper number 2000GC000092 [7490 words, 10 figures, 2 animations, 1 table].

Graham, D., Lupton, J., Albarede, F., Condomines, M., 1990. Extreme temporal homogeneity of helium isotopes at Piton de la Fournaise, Reunion Island. Nature 347, 545–548.

Gurnis, M., Davies, G., 1986. The effect of depth-dependent viscosity on convective mixing in the mantle and the possible survival of primitive mantle. Geophys. Res. Lett. 13, 541–544.

Harper, C.L., Jacobsen, S.B., 1996. Noble gases and Earth's accretion. Science 273, 1814–1818.

Helffrich, G., 2002. Chemical and seismological constraints on mantle heterogeneity. Phil. Trans. R. Soc. Lond. A 360, 2493–2505.

Herzberg, C., Raterron, P., Zhang, J., 2000. New experimental observations on the anhydrous solidus for peridotite KLB-1. Geochem. Geophys. Geosyst. Vol. 1, Paper number 2000GC000089 [4498 words, 7 figures, 4 tables].

Hirth, G., Kohlstedt, D., 1996. Water in the oceanic upper-mantle - implications for rheology, melt extraction and the evolution of the lithosphere. Earth Planet. Sci. Lett. 144 (1–2), 93–108.

Hiyagon, H., Ozima, M., 1986. Partition of noble gases between olivine and basalt melt. Geochim. Cosmochim. Acta 50, 2045–2057.

Hiyagon, H., Ozima, M., Marty, B., Zashu, S., Sakai, H., 1992. Noble gases in submarine glasses from mid-ocean ridges and Loihi seamount: Constraints on the early history of the Earth. Geochim. Cosmochim. Acta 56, 1301–1316.

Hofmann, A.W., 1988. Chemical differentiation of the Earth: the relationship between mantle, continental crust, and oceanic crust. Earth Planet. Sci. Lett. 90, 297–314.

Honda, S., Yuen, D.A., Balachandar, S., Reuteler, D., 1993. 3-Dimensional instabilities of mantle convection with multiple phase-transitions. Science 259, 1308–1311.

Hutchins, K.S., Jakosky, B.M., 1996. Evolution of Martian atmospheric argon: implications for sources of volatiles. J. Geophys. Res. 101, 14933–14949.

Jakosky, B., Jones, J.H., 1997. The history of Martian volatiles. Rev. Geophys. 35, 1–16.

Jeffrey, P.M., Anders, E., 1970. Primordial noble gases in separated meteoritic minerals, I. Geochim. Cosmochim. Acta 34, 1175–1198.

Jochum, K., Hofmann, A.W., Ito, E., Seufert, H.M., et, al., 1983. K, U and Th in mid-ocean ridge basalt glasses and heat production, K/U and K/Rb in the mantle. Nature 306, 431–436.

Kaula, W.M., 1999. Constraints on Venus evolution from radiogenic argon. Icarus 139 (1), 32–39.

Kellogg, L.H., Hager, B.H., van der Hilst, R.D., 1999. Compositional stratification in the deep mantle. Science 283, 1881–1884.

Kiefer, W.S., Hager, B.H., 1991. A mantle plume model for the equatorial highlands on Venus. J. Geophys. Res. 96, 20947–20966.

Kurz, M.D., Jenkins, W.J., Hart, S.R., Clague, D., 1983. Helium isotopic variations in volcanic rocks from Loihi seamount and the island of Hawaii. Earth Planet. Sci. Lett. 66, 388–406.

Matsuda, J.M.S., Ozima, M., Ito, K., Ohtaka, O., Ito, E., 1993. Noble gas partitioning between metal and silicate under high pressures. Science 259, 788–790.

Meibom, A., Anderson, D.L., 2003. The statistical upper mantle assemblage. Earth Planet. Sci. Lett., submitted for publication.

Meibom, A., Anderson, D.L., Sleep, N.H., Frei, R., Chamberlain, C.P., Hren, M.T., Wooden, J.L., 2003. Are high he-3/he-4 ratios in oceanic basalts an indicator of deep-mantle plume components? Earth Planet. Sci. Lett. 208, 197–204.

Moresi, L.N., Solomatov, V.S., 1995. Numerical investigation of 2D convection with extremely large viscosity variations. Phys. Fluids 7, 2154–2162.

Nakagawa, T., Tackley, P.J., 2003. Effects of thermo-chemical mantle convection on the thermal evolution of the earth's core. Earth Planet. Sci. Lett. 220, 107–119.

Namiki, N., Solomon, S.C., 1998. Volcanic degassing of argon and helium and the history of crustal production on venus. J. Geophys. Res 103, 3655–3677.

Ono, S., Ito, E., Katsura, T., 2001. Mineralogy of subducted basaltic crust (MORB) from 25 to 37 GPa, and chemical heterogeneity of the lower mantle. Earth Planet. Sci. Lett. 190, 57–63.

Ozima, M., Kudo, K., 1972. Excess argon in submarine basalts and an earth-atmosphere evolution model. Nature 239, 23–24.

Pepin, R.O., 1991. On the origin and early evolution of terrestrial planet atmospheres and meteoritic volatiles. Icarus 92, 2–79.

Porcelli, D., Halliday, A.N., 1992. The core as a possible source of mantle helium. Earth Planet. Sci. Lett. 192, 45–56.

Porcelli, D., Wasserburg, G.J., 1995. Mass transfer of helium, neon, argon, and xenon through a steady-state upper mantle. Geochimica et Cosmochimica Acta 23, 4921–4937.

Reese, C.C., Solomatov, V.S., Moresi, L.N., 1999. Non-newtonian stagnant lid convection and magmatic resurfacing on Venus. Icarus 139 (1), 67–80.

Ringwood, A.E., 1990. Slab-mantle interactions: 3. petrogenesis of intraplate magmas and structure of the upper mantle. Chem. Geol. 82, 187–207.

Samuel, H., Farnetani, C.G., 2003. Thermochemical convection and helium concentrations in mantle plumes. Earth Planet. Sci. Lett. 207, 39–56.

Sasaki, S., Tajika, E., 1994. Degassing history and evolution of volcanic activities of terrestrial planets based on radiogenic noble gas degassing models. In: Farley, K.A. (Ed.), Volatiles in the Earth and Solar System. AIP Press, New York, pp. 186–199.

Schmalzl, J., Houseman, G.A., Hansen, U., 1996. Mixing in vigorous, time-dependent three-dimensional convection and application to the Earth's mantle. J. Geophys. Res. 101, 21847–21858.

Schott, B., van den Berg, A.P., Yuen, D.A., 2001. Focussed time-dependent Martian volcanism from chemical differentiation coupled with variable thermal conductivity. Geophys. Res. Lett. 28 (22), 4271–4274.

Scott, D.R., Stevenson, D.J., 1989. A self-consistent model of melting, magma migration and buoyancy-driven circulation beneath mid-ocean ridges. J. Geophys. Res. 94, 2973–2988.

Solomatov, V.S., Moresi, L.N., 1996. stagnant lid convection on Venus. J. of Geophys. Res. 101 (E2), 4737–4753.

Stacey, F.D., 1992. Physics of the Earth, third ed. Brookfield, Kenmore, Queensland, Australia, 513 pp.

Steinbach, V., Yuen, D., 1994. Effects of depth-dependent properties on the thermal anomalies produced in flush instabilities from phase transitions. Phys. Earth Planet. Interiors 86, 165–183.

Tackley, P.J., 1996a. Effects of strongly variable viscosity on three-dimensional convection in planetary mantles. J. Geophys. Res 101, 3311–3332.

Tackley, P.J., 1996b. On the ability of phase transitions and viscosity layering to induce long wavelength heterogeneity in the mantle. Geophys. Res. Lett. 23, 1985–1988.

Tackley, P.J., 1998. Three-dimensional simulations of mantle convection with a thermo-chemical basal boundary layer: D"? In: Gurnis, M., Wysession, M.E., Knittle, E., Buffett, B.A. (Eds.), The Core-Mantle Boundary Region. American Geophysical Union, pp. 231–253.

Tackley, P.J., 2000a. Mantle convection and plate tectonics: toward an integrated physical and chemical theory. Science 288, 2002–2007.

Tackley, P.J., 2000b. Self-consistent generation of tectonic plates in time-dependent, three-dimensional mantle convection simulations part 1:pseudo-plastic yielding. Geochem. Geophys. Geosyst. 1, Paper number 2000GC000036 [14,503 words, 21 figures, 1 table].

Tackley, P.J., 2000c. Self-consistent generation of tectonic plates in time-dependent, three-dimensional mantle convection simulations part 2: strain weakening and asthenosphere. Geochem. Geophys. Geosyst. 1, Paper number 2000GC000043 [14,420 words, 15 figures, 1 table].

Tackley, P.J., 2002. Strong heterogeneity caused by deep mantle layering. Geochem. Geophys. Geosyst. 3 (4), 10.1029/2001GC000167.

Tackley, P.J., King, S.D., 2003. Testing the tracer ratio method for modeling active compositional fields in mantle convection simulations. Geochem. Geophys. Geosyst. 4 (4), 8302, doi:10.1029/2001GC000214.

Tackley, P.J., Stevenson, D.J., 1993. A mechanism for spontaneous self-perpetuating volcanism on the terrestrial planets. In: Stone, D.B., Runcorn, S.K. (Eds.), Flow and Creep in the Solar System: Observations, Modeling and Theory. Kluwer Academic Publishers, Dordrecht, pp. 307–322.

Tackley, P.J., Stevenson, D.J., Glatzmaier, G.A., Schubert, G., 1994. Effects of multiple phase transitions in a three-dimensional spherical model of convection in Earth's mantle. J. Geophys. Res 99, 15877–15901.

Tackley, P.J., Xie, S., 2002. The thermochemical structure and evolution of Earth's mantle: constraints and numerical models. Phil. Trans. R. Soc. Lon. A 360 (1800), 2593–2609.

Tackley, P.J., Xie, S., 2003. STAG3D: A code for modeling thermo-chemical multiphase convection in Earth's mantle. In: Bathe, K.J. (Ed.), Proceedings of the Second MIT Conference on Computational Fluid and Solid Mechanics. Elsevier B.V., Amsterdam, 1524–1527.

Turcotte, D.L., Schubert, G., 1988. Tectonic implications of radiogenic noble gases in planetary atmospheres. Icarus 74, 36–46.

Turner, G., 1989. The outgassing history of the earth's atmosphere. J. Geol. Soc. Lond. 146, 147–154.

Van Keken, P.E., 2001. Cylindrical scaling for dynamical cooling models of the Earth. Phys. Earth Planet. Inter. 124, 119–130.

Van Keken, P.E., Ballentine, C.J., 1998. Whole-mantle versus layered mantle convection and the role of a high-viscosity lower mantle in terrestrial volatile evolution. Earth Planet. Sci. Lett. 156, 19–32.

Van Keken, P.E., Ballentine, C.J., 1999. Dynamical models of mantle volatile evolution and the role of phase transitions and temperature-dependent rheology. J. Geophys. Res. 104, 7137–7151.

von Zahn, U., Kumar, S., Niemann, H., Prinn, R., 1983. Composition of the Venus atmosphere. In: Hunten, D.M., Colin, L., Donahue, T.M., Moroz, V.I. (Eds.), Venus. The University of Arizona Press, pp. 299–430.

Weidner, D.J., Wang, Y.B., 1998. Chemical- and clapeyron-induced buoyancy at the 660 km discontinuity. J. Geophys. Res. 103, 7431–7441.

Weinstein, S.A., 1992. Induced compositional layering in a convecting fluid layer by an endothermic phase transition. Earth Planet. Sci. Lett. 113, 23–39.

Zerr, A., Diegeler, A., Boehler, R., 1998. Solidus of Earth's deep mantle. Science 281, 243–246.

Zhong, S., Gurnis, M., 1993. Dynamic feedback between a continent-like raft and thermal convection. J. Geophys. Res. 98 (B7), 12219–12232.